PLASMA-ANODE ELECTRON GUN RESEARCH

R.W Schumacher and J. Santoru
Hughes Research Laboratories
3011 Malibu Canyon Road
Malibu, California 90265

May 1989

F49620-86-C-0105
Final Report
July 15, 1986 through February 15, 1989

Prepared for
AIR FORCE OFFICE OF SCIENTIFIC RESEARCH
Bolling Air Force Base
Washington, DC 20332-6448

Unclassified
SECURITY CLASSIFICATION OF THIS PAGE

REPORT DOCUMENTATION PAGE

Form Approved OMB No. 0704-0188

1a. REPORT SECURITY CLASSIFICATION: Unclassified	1b. RESTRICTIVE MARKINGS
2a. SECURITY CLASSIFICATION AUTHORITY	3. DISTRIBUTION/AVAILABILITY OF REPORT: Approved for Public Release Distribution Unlimited
2b. DECLASSIFICATION/DOWNGRADING SCHEDULE	
4. PERFORMING ORGANIZATION REPORT NUMBER(S)	5. MONITORING ORGANIZATION REPORT NUMBER(S): AFOSR-TR- 89-1190
6a. NAME OF PERFORMING ORGANIZATION: Hughes Research Laboratories; 6b. OFFICE SYMBOL (If applicable)	7a. NAME OF MONITORING ORGANIZATION: Same as 8a
6c. ADDRESS (City, State, and ZIP Code): 3011 Malibu Canyon Rd. Malibu, CA 90265	7b. ADDRESS (City, State, and ZIP Code): Same as 8c
8a. NAME OF FUNDING/SPONSORING ORGANIZATION: Air Force Office of Scientific Research/NP; 8b. OFFICE SYMBOL (If applicable): NP	9. PROCUREMENT INSTRUMENT IDENTIFICATION NUMBER: F49620-86-C0105
8c. ADDRESS (City, State, and ZIP Code): Bolling Air Force Base, Bldg.410 Washington, DC 20332-6448	10. SOURCE OF FUNDING NUMBERS: PROGRAM ELEMENT NO. 61102F; PROJECT NO. 2301; TASK NO. A8; WORK UNIT ACCESSION NO.

11. TITLE (Include Security Classification): PLASMA-ANODE ELECTRON GUN RESEARCH (U)

12. PERSONAL AUTHOR(S): Robert W. Schumacher and Joseph Santoru

13a. TYPE OF REPORT	13b. TIME COVERED	14. DATE OF REPORT (Year, Month, Day)	15. PAGE COUNT
FINAL	FROM 7/15/86 TO 2/15/89	1989 May 30	61

16. SUPPLEMENTARY NOTATION

17. COSATI CODES			18. SUBJECT TERMS (Continue on reverse if necessary and identify by block number)
FIELD	GROUP	SUB-GROUP	Electron Sources; Microwave Generation; Electron Beams; Bennett Pinch; Beam Weapons; Cold Cathodes

19. ABSTRACT (Continue on reverse if necessary and identify by block number)

The plasma-anode electron gun (PAG) is a new cold-cathode electron source which exhibits many novel features. These include instant starting, no cathode heater power, minimal vacuum requirements, a nonpoisoning cathode, long-pulse operation without gap closure, and beam modulation at ground potential with constant beam energy. The basic concept involves a collective interaction between counterpropagating streams of electrons and ions in a high-voltage diode gap. A Pierce electron-gun configuration is employed, but the thermionic cathode is replaced with a cold, secondary-electron-emitting electrode. Electron emission is stimulated by bombarding the cathode with high-energy ions. The ions are injected into the high-voltage gap through a gridded structure from a plasma source, which is embedded inside the anode electrode. The gridded structure serves as both a cathode for the plasma discharge and as an anode for...

(over)

20. DISTRIBUTION/AVAILABILITY OF ABSTRACT	21. ABSTRACT SECURITY CLASSIFICATION
☐ UNCLASSIFIED/UNLIMITED ☑ SAME AS RPT. ☐ DTIC USERS	Unclassified
22a. NAME OF RESPONSIBLE INDIVIDUAL: Dr Robert Barker	22b. TELEPHONE (Include Area Code): (202) 767-5011; 22c. OFFICE SYMBOL: NP

DD Form 1473, JUN 86 — Previous editions are obsolete. — SECURITY CLASSIFICATION OF THIS PAGE

Unclassified

Unclassified

SECURITY CLASSIFICATION OF THIS PAGE

19. Abstract (Continued)

the PAG. As high-voltage ions impact the cathode surface, secondary electrons are emitted, accelerated back through the diode gap, and focused through an on-axis aperture in the anode.

Under this program, a modified Herrmannsfeldt computer code was constructed that calculates electron and ion trajectories and limiting particle currents in realistic geometries in the self-consistent space-charge fields of both particle species. This code was used to design a 120-kV PAG scaling experiment. Construction of the new experiment was completed and operation was achieved at gun voltages up to 100 kV. The PAG demonstrated square-wave, 17-μs-long beam pulses at 100 kV and 10 A. Stable gun operation has also been demonstrated at 70 kV and 2.5 A for 210-μs pulse lengths without gap closure. The beam profile is consistent with beam transport via ion focusing by the background plasma and the Bennett pinch. A perpendicular beam temperature of 15 eV is inferred by comparing the measured 7-mm-diameter beam with a Bennett profile fit. Scaling of the beam current with incident ion flux indicates that the beam current is ultimately limited by ion space charge at the anode. Broad wings are observed on the beam profile when the PAG gap is operated beyond the ion-space-charge current-limited regime. Scaling of the secondary-electron yield with gap voltage has demonstrated yields up to 13 at 100 kV. An independent electron-beam temperature diagnostic was used to measure the transverse beam temperature. The temperature was in good agreement with the estimate obtained from the Bennett-profile fit.

The maximum beam current that can be extracted from the PAG is ultimately determined by the space-charge-limited ion current that flows in the diode gap. To increase the electron-beam current density beyond this limit, we developed the Hollow-Cathode-Plasma (HCP) E-gun under our separate IR&D project on Pulsed Power Switches for Military Systems. The HCP E-gun exploits a low-pressure glow discharge inside a hollow-cathode enclosure to generate a stable high-density plasma from which a high-current-density E-beam can be extracted. Under our IR&D project we developed HCP E-guns that produce up to 40 A/cm^2 in a circular cross-section. With the consent of the Air Force, we adapted the new HCP E-gun configuration to the requirements of our parallel Plasma Three-Wave-Mixing Program (Air Force Office of Scientific Research Contract No. F49620-85-C-0059) under the present PAG contract. The Three-Wave-Mixing program was previously using planar PAG guns and millimeter-wave power scaling experiments with beam current were limited to only 7 A of total injected beam current. The adapted HCP E-guns have enabled the E-gun current to reach the 100-A (20-A/cm^2) level with 13-μs-long pulses at 30 kV of beam voltage.

Unclassified

SECURITY CLASSIFICATION OF THIS PAG

TABLE OF CONTENTS

LIST OF ILLUSTRATIONS

LIST OF ILLUSTRATIONS (Continued)

SECTION 1

INTRODUCTION

This final report documents research performed under AFOSR contract No. F49620-86-C-0105, which is entitled, "Plasma-Anode Electron Gun Research." Under this program, a modified Herrmannsfeldt computer code[1] was constructed that calculates electron and ion trajectories and limiting particle currents in realistic geometries in the self-consistent space-charge fields of both particle species. This code was used to design a 120-kV plasma-anode electron gun (PAG) scaling experiment. Construction of the new experiment was completed and operation was achieved at gun voltages up to 100 kV. The PAG has demonstrated square-wave, 17-μs-long beam pulses at 100 kV and 10 A. Stable gun operation has also been demonstrated at 70 kV and 2.5 A for 210-μs pulse lengths without gap closure. The beam profile is consistent with beam transport via ion focusing by the background plasma and the Bennett pinch. A transverse beam temperature of 15 eV was inferred by comparing the measured 7-mm-diameter beam with a Bennett-profile fit. Scaling of the beam current with incident cathode-ion flux indicates that the beam current is ultimately limited by ion space charge at the anode. Broad wings are observed on the beam profile when the PAG gap is operated beyond the ion-space-charge current-limited regime. Scaling of the secondary-electron yield with gap voltage has demonstrated yields up to 13 at 100 kV. An independent electron-beam (E-beam)

temperature diagnostic was used to measure the transverse temperature. The temperature was in good agreement with the estimate obtained from the Bennett-profile fit.

The PAG is an original Hughes concept[2] that maintains many novel features, including:

- Instant starting
- No cathode heater
- Nonpoisoning cathode
- Minimal vacuum requirements
- Long-pulse operation without gap closure
- High brightness
- Beam modulation with low power at ground potential
- Constant beam energy

Figure 1 illustrates the basic concept, which involves a collective interaction between counterpropagating streams of electrons and ions in a high-voltage diode gap. A Pierce electron-gun[3] configuration is employed, but the thermionic cathode is replaced with a cold, secondary-electron-emitting electrode. Electron emission is stimulated by bombarding the cathode with high-energy ions. The ions are injected into the high-voltage gap through a gridded structure from a plasma source, which is embedded inside the anode electrode. The gridded structure serves as both a cathode for the plasma discharge and as an anode for the PAG. The plasma can be

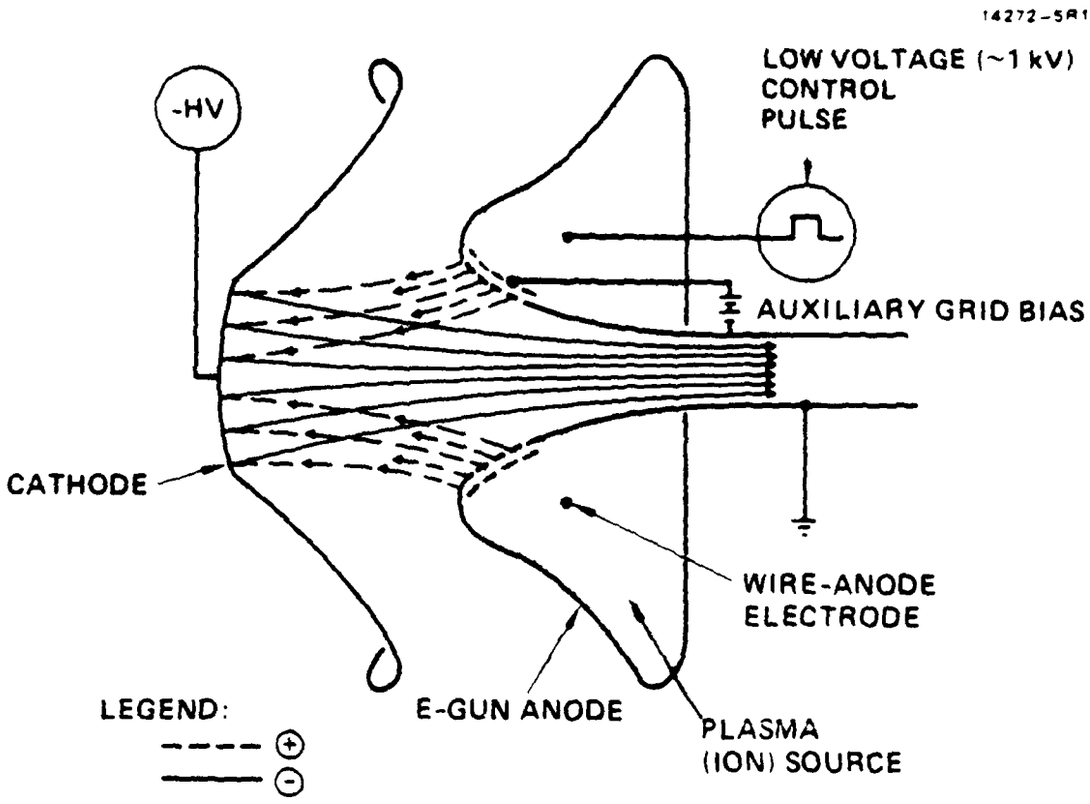

Figure 1. Plasma-anode E-gun (PAG) concept.

generated by various means, but the preferred approach is to use a wire-anode glow discharge[4,5] at low gas pressure (<50 mTorr). As high-voltage ions impact the cathode surface, secondary electrons are emitted and accelerated back through the diode gap. If the proper electrode configuration is chosen (which accounts for electron and ion space-charge in a self-consistent manner) then electrostatic fields can be generated that focus the electrons through the on-axis aperture in the anode to form a laminar beam with a uniform circular cross section.

Since gas from the plasma source in the anode may pass into the high-voltage gap, the operating point of the gap must be chosen so as to standoff high voltage against both vacuum- and Paschen-breakdown mechanisms (as shown in Figure 2). This selected operating point limits the voltage per gap to typically 200 kV. Beam acceleration to higher voltages can be accomplished with multiple gaps.

Because the pressure limit is imposed by Paschen breakdown, helium gas is usually employed since it provides the highest voltage holdoff against Paschen breakdown relative to any other gas. Published data,[6] data obtained in the Hughes E-beam controlled switch[7] (developed under Air Force contract No. F33615-81-C-2009), and data obtained under this contract indicate that a secondary-electron yield of 13 to 15 is obtained for 100-keV helium-ion impact upon molybdenum surfaces in the presence of a background helium gas.

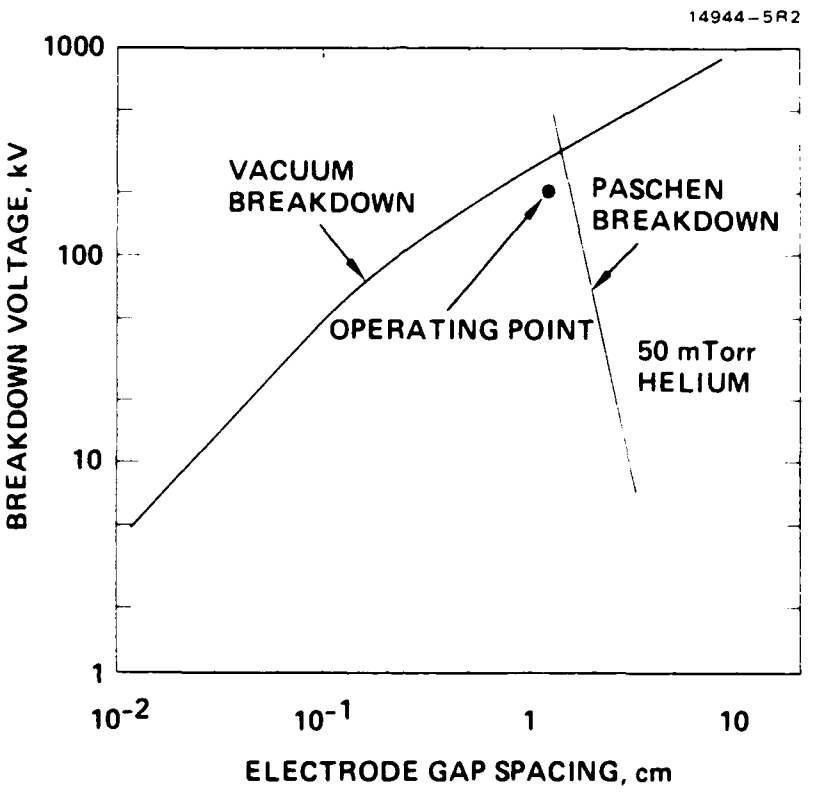

Figure 2. Typical operating point of a PAG high-voltage gap.

The E-beam current in the PAG is controlled at low voltage by modulating the (~1 kV) wire-anode discharge at the ground-potential environment of the anode electrode. Since the plasma is confined within the gridded anode structure (the electrons cannot penetrate into the anode-cathode gap because of the high electron-repelling E-gun potential), plasma closure of the high-voltage gap cannot occur and long-pulse (>>1 μs) operation is achieved. Modulation of the plasma source modulates the ion flux incident upon the cathode which, in turn, controls the beam current. A monoenergetic beam is obtained throughout the beam pulse because the E-beam is switched ON and OFF by the plasma source and not by the high-voltage supply for the cathode. Low-energy electrons, which result from the rise and fall of the cathode voltage in conventional pulsed beams, will not be present. All of this is accomplished without heater power and without high-vacuum-environment requirements because the ordinary-metal cathode used in the PAG cannot be poisoned.

The maximum beam current that can be extracted from the PAG is ultimately determined by the space-charge-limited ion current that flows in the diode gap. To increase the electron-beam current density beyond this limit, we developed the Hollow-Cathode-Plasma (HCP) E-gun under our separate IR&D project on Pulsed Power Switches for Military Systems. The HCP E-gun exploits a low-pressure glow discharge inside a hollow-cathode enclosure to generate a stable high-density plasma from which a

high-current-density E-beam can be extracted. Under our IR&D project we developed HCP E-guns that produce up to 40 A/cm^2 in a circular cross-section. With the consent of the Air Force, we adapted the HCP E-gun configuration to the requirements of our parallel Plasma Three-Wave-Mixing Program (AFOSR Contract No. F49620-85-C-0059) under the present PAG contract. The Three-Wave-Mixing Program was previously using planar PAG guns and millimeter-wave power scaling experiments with beam current were limited to only 7 A of total injected beam current. The adapted HCP E-guns have enabled the E-gun current to reach the 100-A (20-A/cm^2) level with 13-μs-long pulses at 30 kV of beam voltage.

Development of the plasma-anode electron-gun (E-gun) and the HCP E-gun may have a significant impact on many important high-power Air Force systems. For example, they may improve the performance and decrease the auxiliary power requirements of conventional devices, such as klystrons and traveling-wave tubes, that are presently deployed on aircraft and satellites. These E-guns may also provide one of the key enabling technologies required for new Air Force systems, such as free-electron lasers, high-power excimer lasers, and E-beam weapons.

SECTION 2

PLASMA-ANODE E-GUN CALCULATIONS AND EXPERIMENTS

In this section we discuss our progress in computer-code development and application, PAG scaling experiments, beam profile measurements, and beam-temperature-diagnostic systems.

2.1 COMPUTER-CODE DEVELOPMENT AND APPLICATION

We have developed and applied new computer programs that are capable of computing the trajectories of electrons and ions through the PAG in the self-consistent space-charge field of both species. Realistic boundary and electrode potentials are used as input data. Under a separate contract with Hughes, which was supported by IR&D funds, Dr. W. Herrmannsfeldt of Stanford University revised an earlier version of his electron trajectories code to self-consistently compute the trajectories and space-charge fields of more than one charged species in an E-gun, with each species having an arbitrarily specified charge-to-mass ratio. The code was adapted for the VAX 11/785 and 8650 computers at Hughes Research Laboratories (HRL).

An electron-generation code that supports the new Herrmannsfeldt program was also constructed. The function of this latter code is to iteratively generate the initial conditions for the electrons at the cathode surface by multiplying the local ion flux at the cathode by the appropriate secondary-emission coefficient.

The new Herrmannsfeldt code maintains the versatility of the original code. For example, the number of iterations on the space-charge computation can be reduced to one to simulate space-charge neutralization (i.e., remove the self-consistent space-charge field) by plasma in specified regions of some PAG designs.

This versatility was exploited when the code was used to design the 120-kV PAG scaling experiment. Many different code runs were completed in order to arrive at an optimal PAG design. During the course of these runs it became evident that the new code was revealing important physics that we were not able to see using an earlier single-species code. One of the most important features that was revealed was a reduction in the electron emittance which was made possible by the presence of the ion space charge. This effect is illustrated dramatically by the runs shown in Figure 3 for the experimental PAG operating at 80 kV and 10 A. The two trajectory plots show the transport of electrons with identical initial conditions, but with [Figure 3(a)] and without [Figure 3(b)] the presence of positive helium ions. E-beam focusing and collimation are greatly assisted by the presence of the ion space charge. Perturbation analyses of these trajectories reveal that the greatest influence of the ion space charge is near the cathode where the electron velocities are small.

2.2 120-kV PAG SCALING EXPERIMENT

The second task in the PAG program was the design, fabrication, and operation of a 120-kV PAG scaling experiment. In

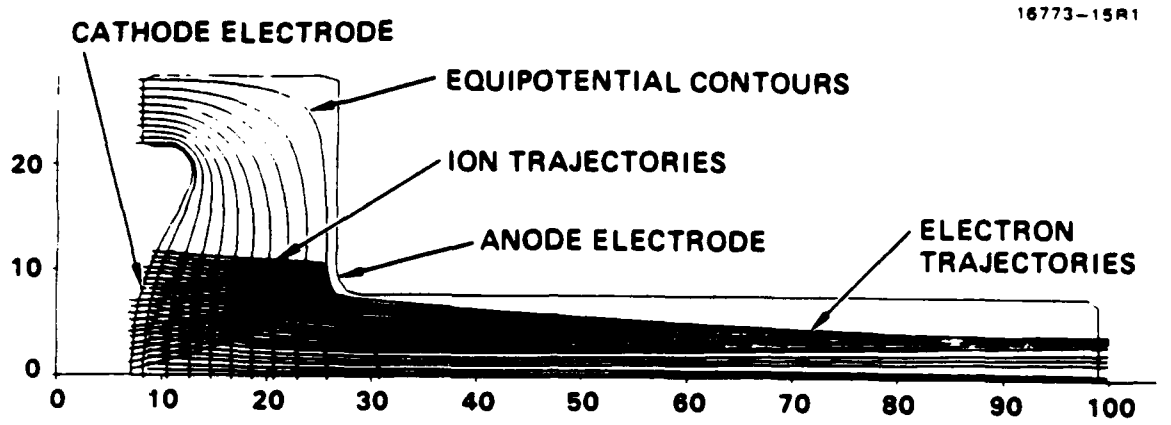

(a)

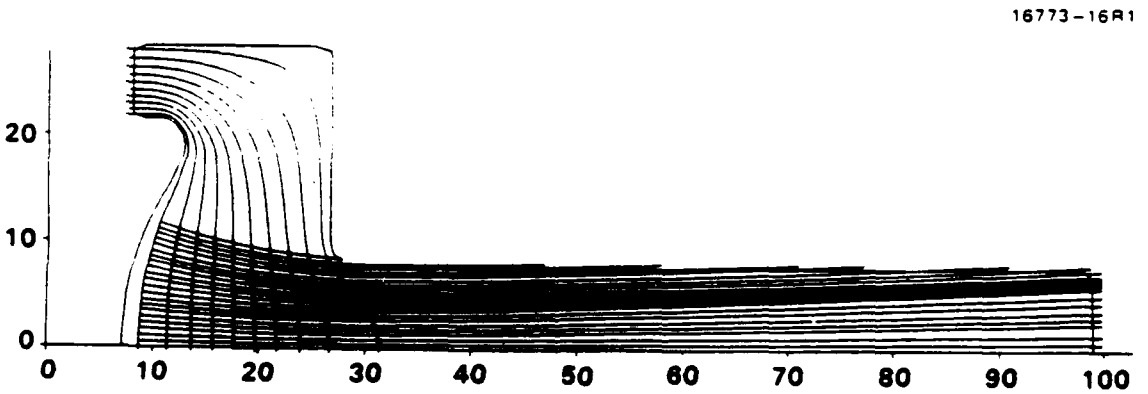

(b)

Figure 3. Modified Hermannsfeldt-code runs at 80 kV and 10 A showing electron trajectories with (a) and without (b) the presence of ions in the gap.

this section we describe the experimental apparatus, beam current and voltage scaling, E-beam profiles, and beam temperature diagnostics and measurements.

2.2.1 Experimental Apparatus and Diagnostics

The 120-kV PAG scaling experiment is shown schematically in Figure 4 and in a photograph in Figure 5. The experiment was designed to compare actual PAG data with code predictions and to investigate E-beam quality at voltage and current up to 120 kV and 18 A. The detailed geometry of the high-voltage gap was determined using the modified Herrmannsfeldt code described earlier. Figure 3(a) shows the diode configuration used, together with equipotential contours and ion and electron trajectories for a 10-A E-beam with an energy of 80 kV. The optimum cathode radius of curvature was found to be 5.0 cm for these parameters. The anode-grid electrode was chosen to be planar to facilitate Langmuir-probe access to the low-voltage portion of the gap. A photograph of the completed molybdenum cathode and field-shaping electrodes mounted on the high-voltage dielectric bushing is shown in Figure 6. The bushing is terminated on a 6-in. conflat flange that allows the cathode to be precisely positioned inside the 4-in.-diameter stainless-steel vacuum chamber. An RG-220/U high-voltage coax cable (shown to the right in Figure 5) feeds the cathode through an oil-filled high-voltage connector at the rear of the bushing.

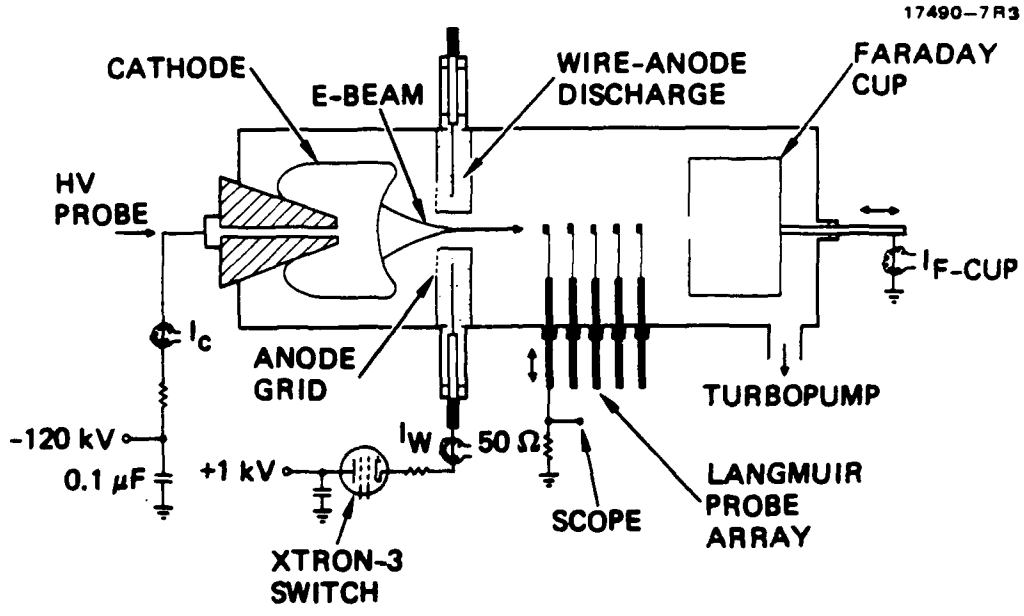

Figure 4. 120-kV PAG-scaling experiment.

MC 17241

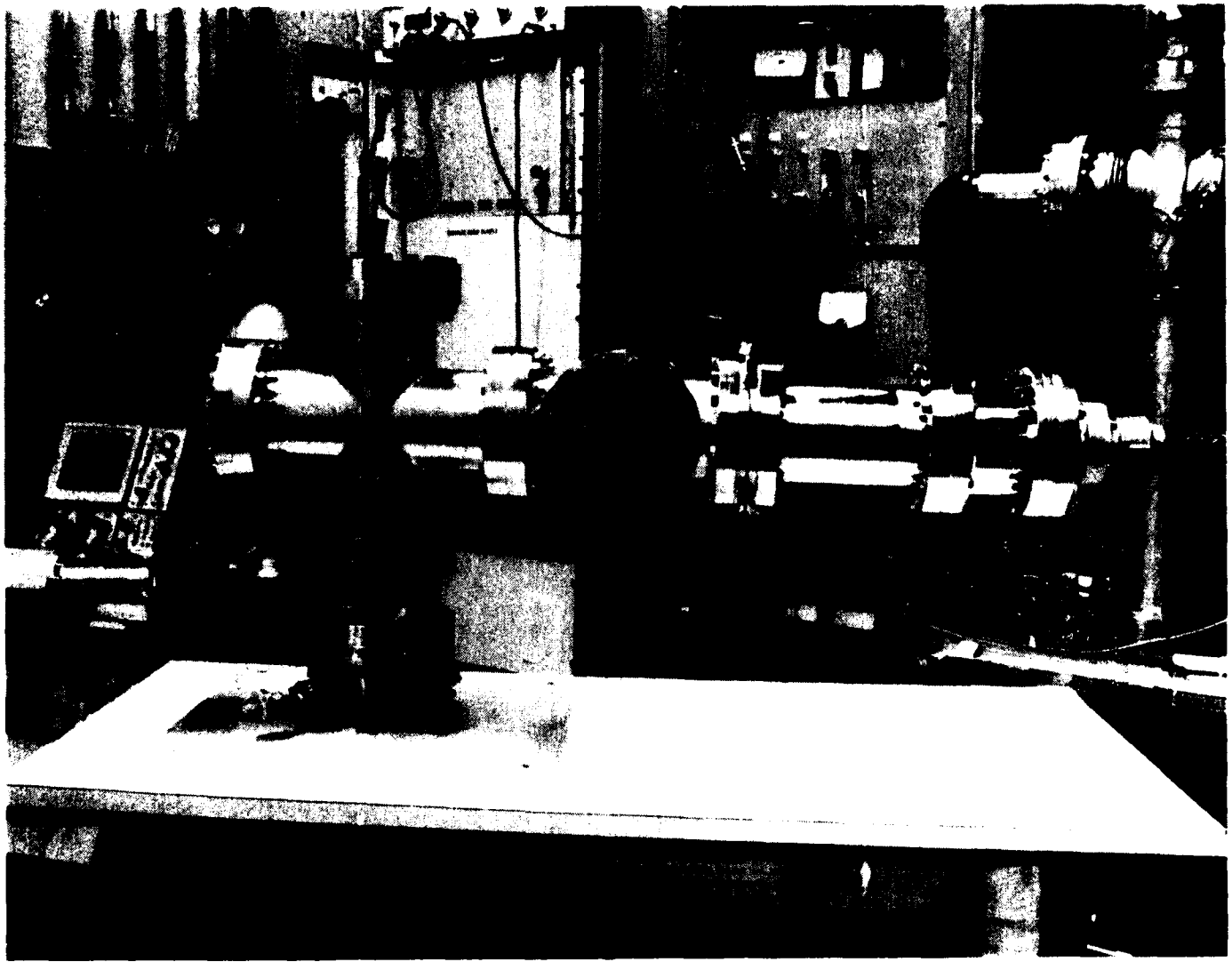

Figure 5. Photograph of the 120-kV PAG scaling experiment.

MC 17240

Figure 6. Photograph of the PAG cathode and high-voltage-bushing assembly.

A wide range of diagnostic equipment has been designed and assembled for the experiment. Electrical diagnostics consist of voltage dividers to measure the cathode and ion-source voltages, and current transformers to measure the cathode, E-beam, and ion-source currents. A three-dimensional probe array has been constructed to measure the beam profiles and divergence angle, and a Faraday cup has been constructed to measure the total beam current. As shown in Figure 4, the Faraday cup can be positioned just downstream of the anode assembly to intercept the entire beam envelope. The cup is moved further downstream when probe measurements are made. A "beam-slit shadowgraph" was used with the probe array to measure the parallel beam temperature.

The E-beam diagnostics discussed above are mounted on the two, four-way conflat-flange crosses shown in Figure 5. This arrangement offers optimum flexibility and diagnostic access to the E-beam. The experiment is evacuated by a turbomolecular pump to avoid the surface-contamination problems associated with diffusion pumps. The helium gas pressure is regulated in the range of 10 to 50 mTorr by flowing gas into the system through a leak valve.

2.2.2 PAG Operation

The experimental PAG has demonstrated well-collimated, high-quality beams in good agreement with the predictions of the modified Herrmannsfeldt code. The E-beam was focused electrostatically by the diode geometry to form a 7-mm-diameter

collimated beam, which was transported over the 1-m length of the experiment without the aid of magnetic-focusing fields. Figure 7 is a photograph of the beam operating continuously at 40 kV and 10 mA. The photograph was taken through a Pyrex window mounted on one of the four-way crosses shown in Figure 5. The path of the narrow beam is indicated by optical line radiation emitted by neutral atoms that are excited by the beam.

Figure 8 shows oscilloscope waveforms for a 17-μs-wide pulse with a beam voltage of 100 kV. The ion-source discharge current was modulated at 100 A using the CROSSATRON^R switch as shown in Figure 4. The discharge generated 10 A of cathode current, which is the sum of the E-beam and incident-ion currents. In this case the Faraday cup collected 8 A of beam current. We have also demonstrated stable PAG operation with ultrawide beam pulses without high-voltage-gap closure. Figure 9 shows operation with pulse widths of 210 μs at 2.5 A of Faraday-cup current at 70-kV beam voltage. The droop in the current waveforms in Figure 9 is caused by the voltage droop in the capacitor bank supplying the ion-source discharge current and is not a feature of the PAG. The droop can be eliminated by simply increasing the size of the capacitor bank.

2.2.3 Parameter Scaling

In these experiments we measured the scaling of Faraday-cup and cathode currents with ion-source discharge current and the beam voltage. We found that the E-beam current is ultimately

MC 17243

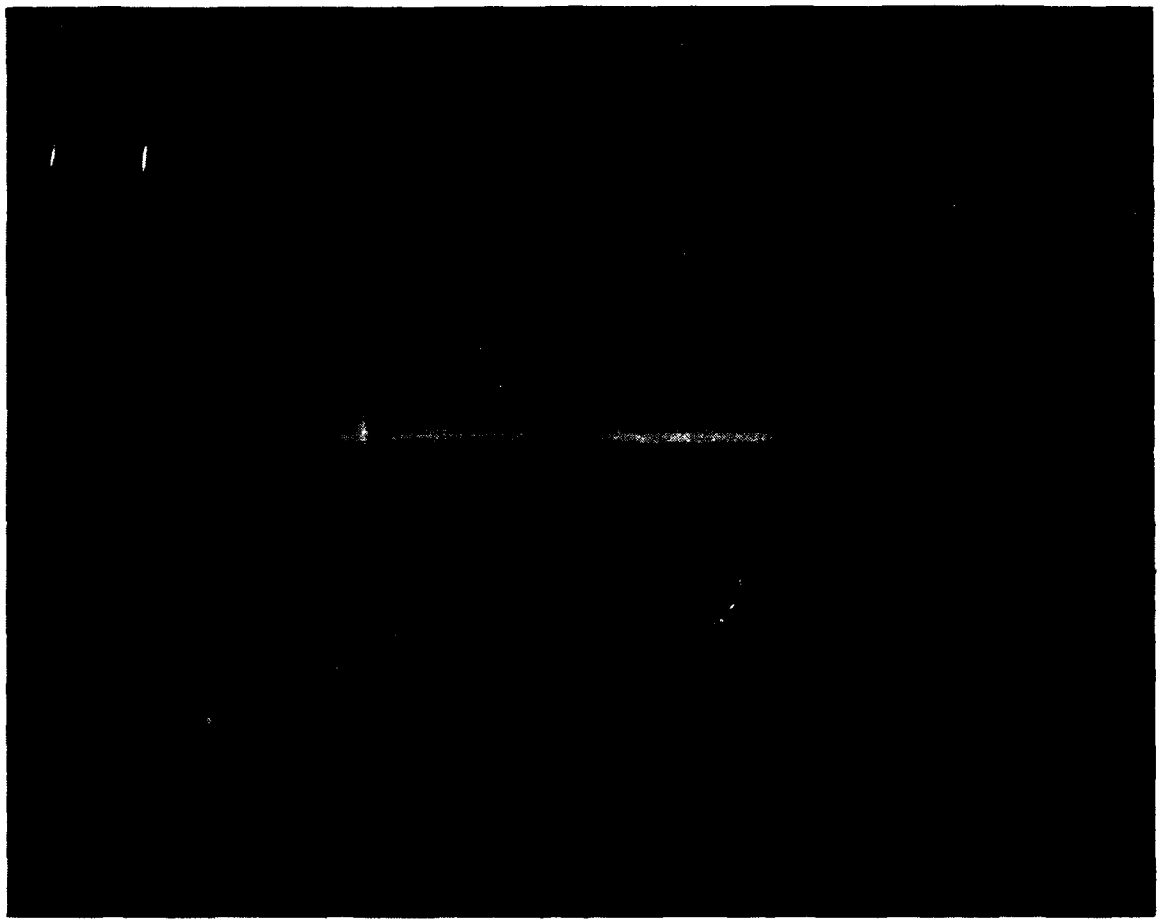

Figure 7. Photograph of narrow 5-mm-diameter PAG beam operating cw at 40 kV and 10 mA.

17325-2

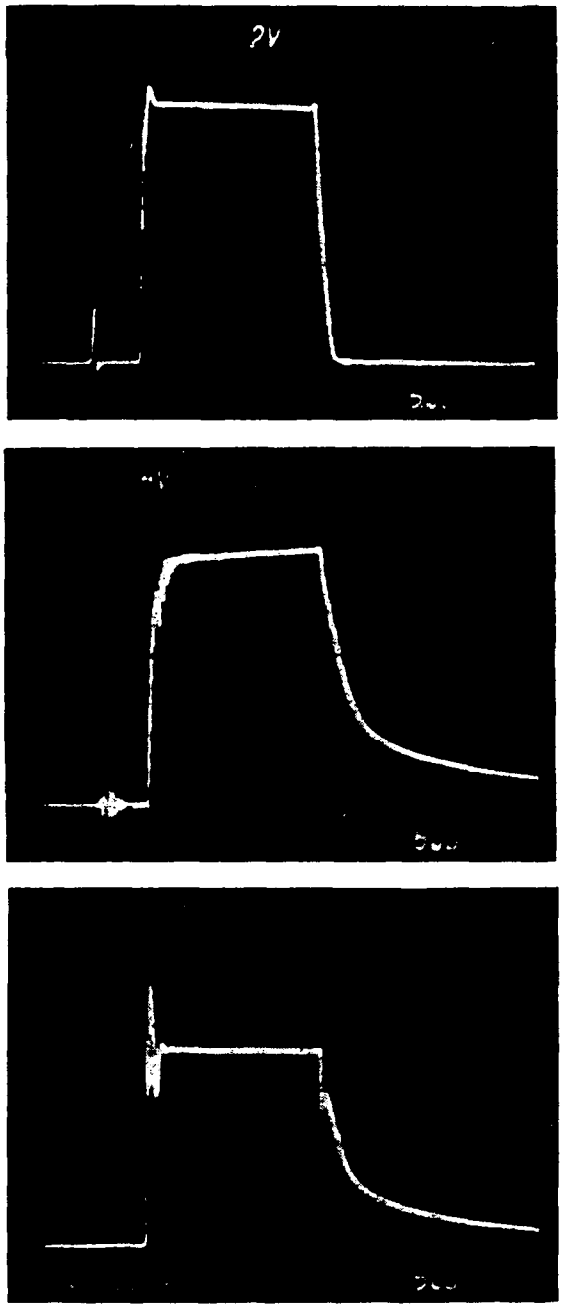

Figure 8. Pulsed PAG operation demonstrating 10 A of cathode current at 100 kV.

17325–3

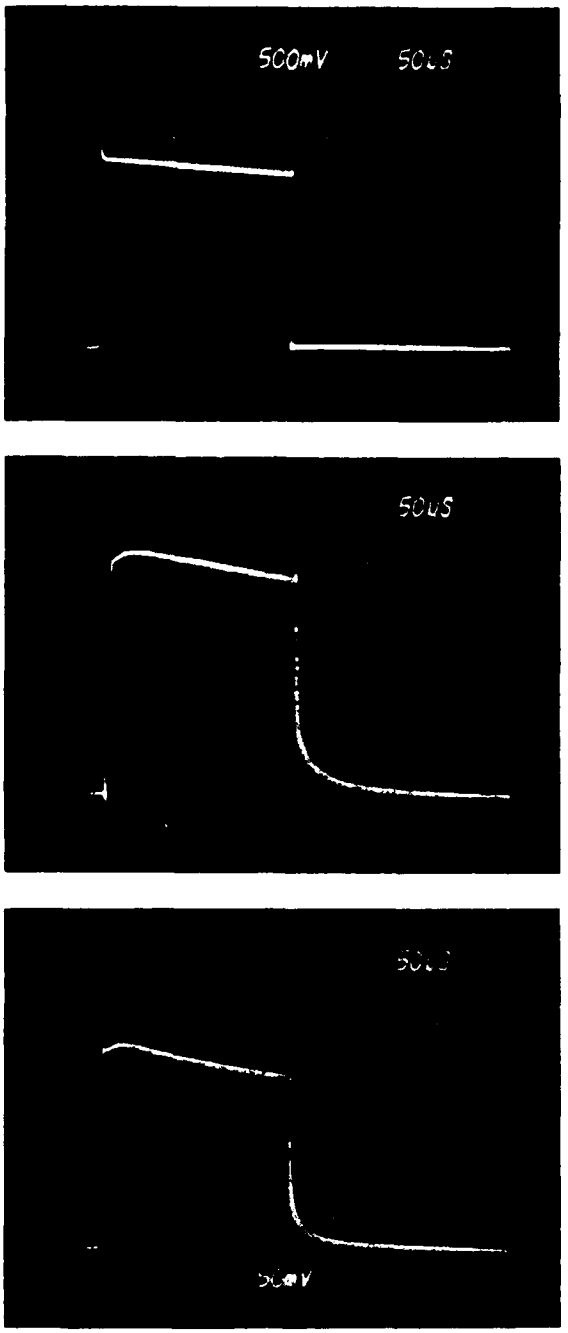

ION-SOURCE
DISCHARGE CURRENT
5 A/div

CATHODE CURRENT
0.5 A/div

FARADAY-CUP
CURRENT
0.5 A/div

TIME, 50 µs/div

Figure 9. PAG operation with 210-µs pulse length.

limited by ion space charge at the anode. Figure 10 shows the scaling of cathode and Faraday-cup currents with ion-source discharge current over the 9 to 100 A range at a constant beam voltage of 90 kV. Both the cathode and Faraday-cup currents increase linearly until the discharge current reaches 30 A. Beyond this point the currents increase at much slower rates. This behavior is also shown in Figure 11, which is the same scaling, but recorded for a lower beam voltage of 50 kV. As the discharge current is increased beyond 20 A, the Faraday-cup current reaches a saturated value of 2 A, while the cathode current continues to increase.

The change in slope of the Faraday-cup and cathode currents is caused by the limitation of ion current incident on the cathode; for normal operation of the PAG, the ion current is restricted to its space-charge-limited value at the anode grid where ions are extracted into the gap. We can estimate the ion-space-charge-limited cathode current using a planar diode approximation for the PAG gap. The expression for Child-Langmuir space-charge-limited current in a planar diode is

$$I = \frac{4}{9} \epsilon_o \left(\frac{2e}{m}\right)^{1/2} \frac{V^{3/2} A}{d^2} \quad , \qquad (1)$$

where V is the gap voltage, d is the gap spacing, A is the emitting surface area, e/m is the charge to mass ratio, and ϵ_o is the permittivity of free space. Since the space-charge-limited

17328-1

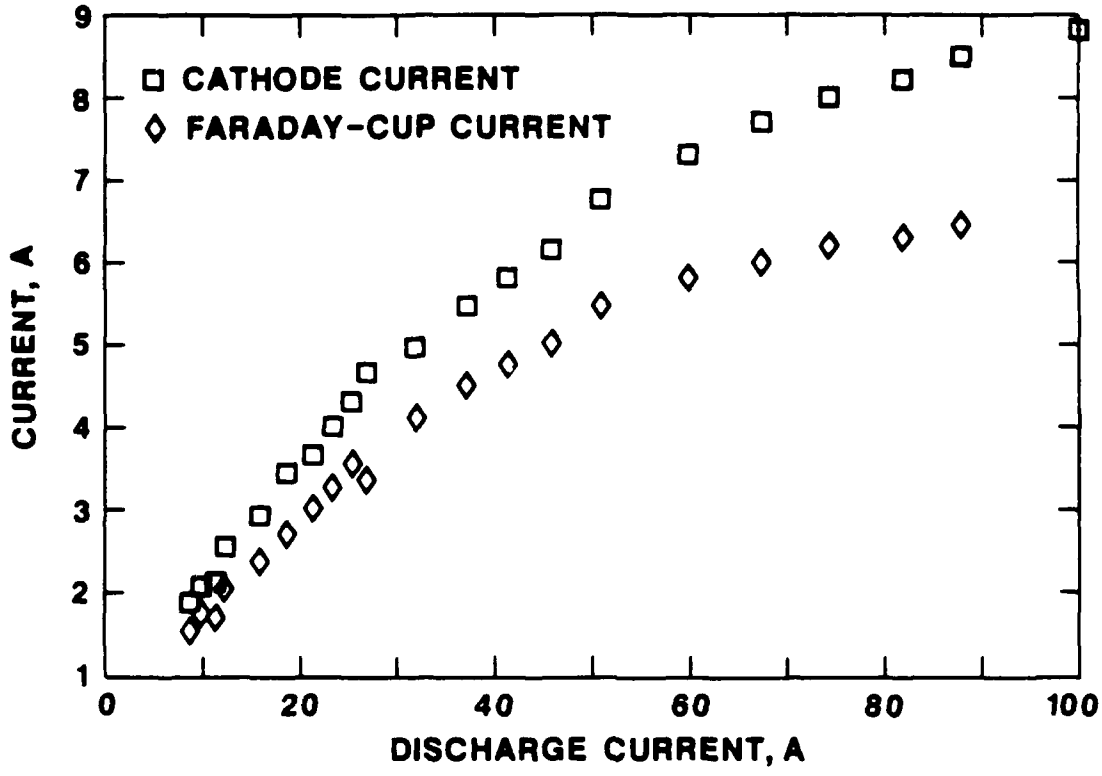

Figure 10. Cathode and Faraday-cup current scaling with ion-source discharge current. V_b = 90 kV.

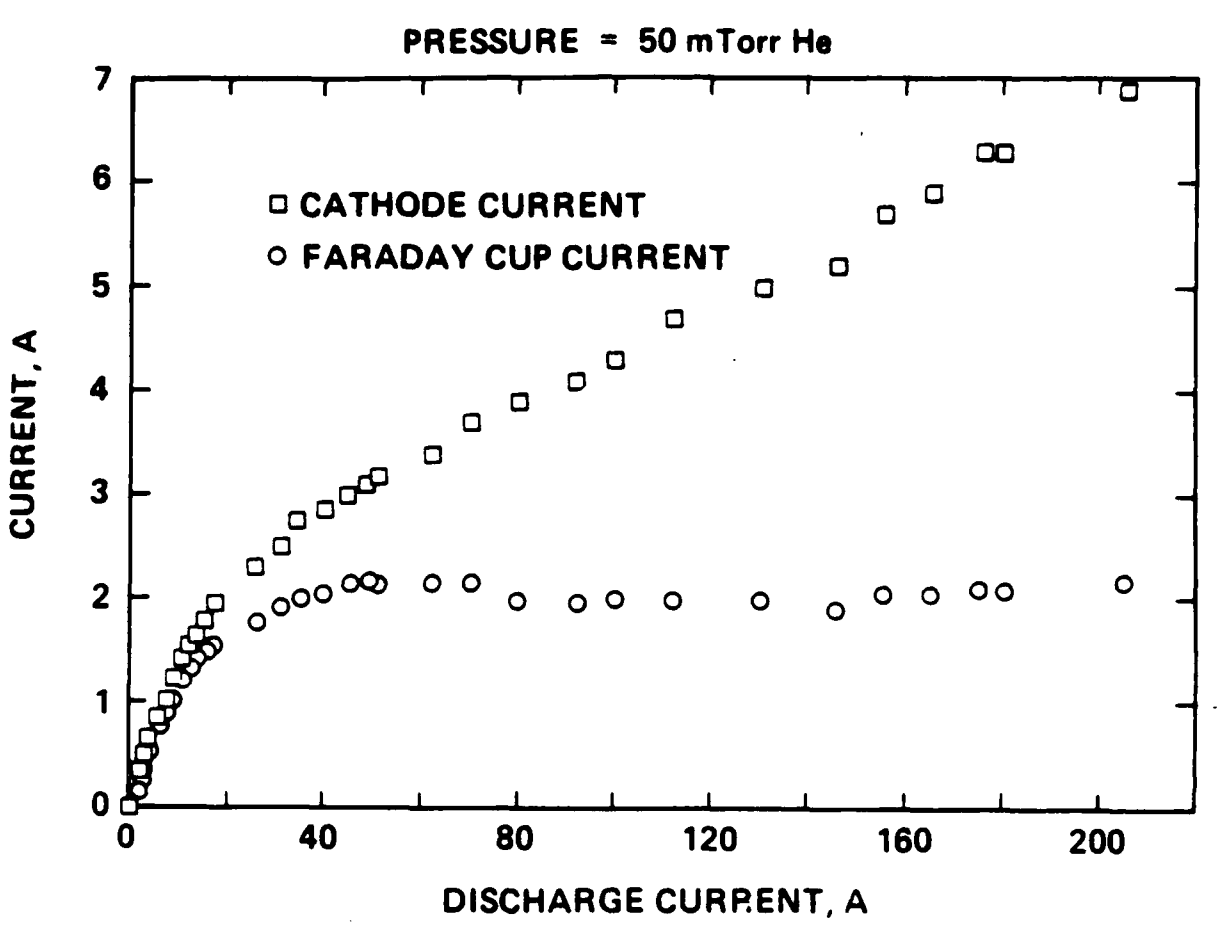

Figure 11. Cathode and Faraday-cup current scaling with ion-source discharge current at V_b = 50 kV.

current scales as $m^{-1/2}$, ion emission at the anode will become space-charge limited well before electron emission at the cathode. For singly charged helium ions, the space-charge-limited ion current is

$$I_i = 2.72 \times 10^{-8} \frac{V^{3/2} A}{d^2} \quad . \tag{2}$$

The total cathode current is the sum of the ion and E-beam currents, or

$$I_c = I_i + I_b \quad . \tag{3}$$

But the electron-beam current can be expressed in terms of the incident ion current and the secondary yield, γ, as

$$I_b = \gamma I_i \quad . \tag{4}$$

Combining Eqs. (2), (3) and (4), the saturated cathode current is

$$I_{c_\ell} = 2.72 \times 10^{-8} \frac{(\gamma+1) V^{3/2} A}{d^2} \quad . \tag{5}$$

Using the PAG experiment parameters A = 3.8 cm^2, d = 3.3 cm, V_b = 90 kV, and γ = 13, Eq. (5) predicts a saturated cathode current of 3.6 A.

The observed linear scaling of cathode current with ion-source discharge current in Figure 10 shows the saturation to begin at the slightly higher value of 4.7 A. This correspondence is sufficiently close considering the level of approximation which does not include the geometrical enhancement of ion perveance resulting from the nonplanar gap configuration. At the lower beam voltage of 50 kV, the cathode current begins to saturate (Figure 11) at a lower value (~1.9 A) which is consistent with the ion-space-charge-limited voltage scaling predicted by Eq. (5).

As the discharge current is increased beyond I_{c_ℓ} in Figures 10 and 11, the cathode current continues to increase. This is due to penetration of the ion-space-charge cloud at the anode into the high-voltage gap; a phenomena which reduces the effective cathode-to-anode spacing (i.e., $d < 3.3$ cm), increases the ion-emitting area, and thereby increases I_{c_ℓ}. Although the cathode current continues to increase, the Faraday-cup current approaches a constant value in Figures 10 and 11. The Faraday cup, therefore, does not collect all the beam current which is generated in this regime; an observation which suggests that the beam becomes defocused when the gap is operated beyond the ion-space-charge limit. Beam profiles presented in the next section verify that this is indeed the case. The beam defocusing is caused by the release of ions from the extended ion space charge cloud at the anode. Ions from the edge of expanded cloud are released on trajectories which map onto the cathode surface at

large radii from the PAG axis. These ions stimulate the emission of secondary electrons (at large radii on the cathode) which are over focused and cross the gun axis thus creating a "halo" or broad wings on the beam profile.

Finally, by comparing the cathode and Faraday-cup currents at each beam voltage we can deduce the secondary electron yield using the equation

$$\gamma = I_b/(I_b + I_c) \quad , \tag{6}$$

which is derived by combining Eqs. (3) and (4). Figure 12 shows the computed electron yield per ion to scale up a value of 13 at voltages up to 100 kV. This plot was prepared by assuming that all the beam current is collected by the Faraday cup. However, since the discharge current was 21 A for this experiment, the PAG was operating in the ion-space-charge current-limited mode for voltages less than 50 kV (as shown in Figure 11). Below 50 kV, therefore, the measured yields are smaller than those actually obtained since some portion of the beam falls outside the Faraday-cup entrance aperture in this regime.

2.2.4 Electron-Beam Profiles

Radial beam profiles were measured using the array of disk probes shown in Figure 4. The probe current was measured at each radial position using the θ = 0° and 90° probe orientations as

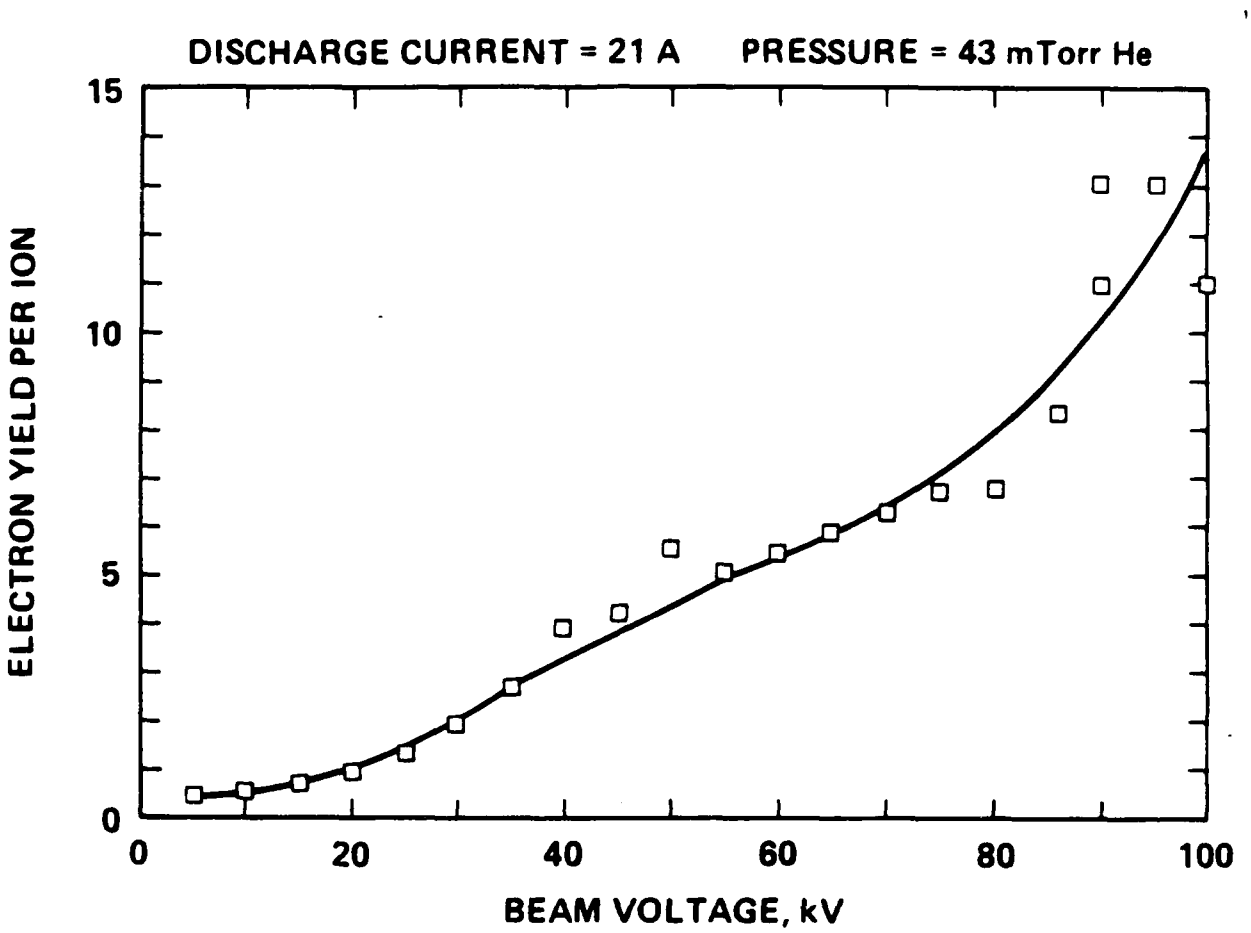

Figure 12. Electron yield per ion as a function of beam voltage.

indicated in Figure 13. At 90° the probe current is largely background-plasma electron current. By subtracting the current measured at 90° from that measured at 0°, we eliminate the background plasma contribution to the beam-probe current. A beam profile measured by slowly scanning the probe across the beam channel is shown in Figure 14. A rather narrow well-collimated, 7-mm-diameter (FWHM) beam was found at 67 kV and 3 A of cathode current.

The beam profile was found to be consistent with beam collimation via ion focusing and the Bennett-pinch effect. As the E-beam propagates through the background helium gas, a tenuous plasma is generated by electron-neutral collisions. Ions in this plasma neutralize the space-charge in the beam and allow it to propagate free of space-charge blow-up effects. However, rather than simply drifting in a ballistic manner, the beam is also subject to the magnetic "pinch" force from the poloidal magnetic field produced by the beam current. This force will constrict the beam channel if the magnetic-field pressure exceeds the transverse thermal beam pressure as shown schematically in Figure 15. This phenomena is known as the Bennett-pinch effect.[8] Quantitatively, the pinch condition may be expressed as

$$\frac{B_p^2}{8\pi} \geq n_b \, T_{b_\perp} \, , \tag{7}$$

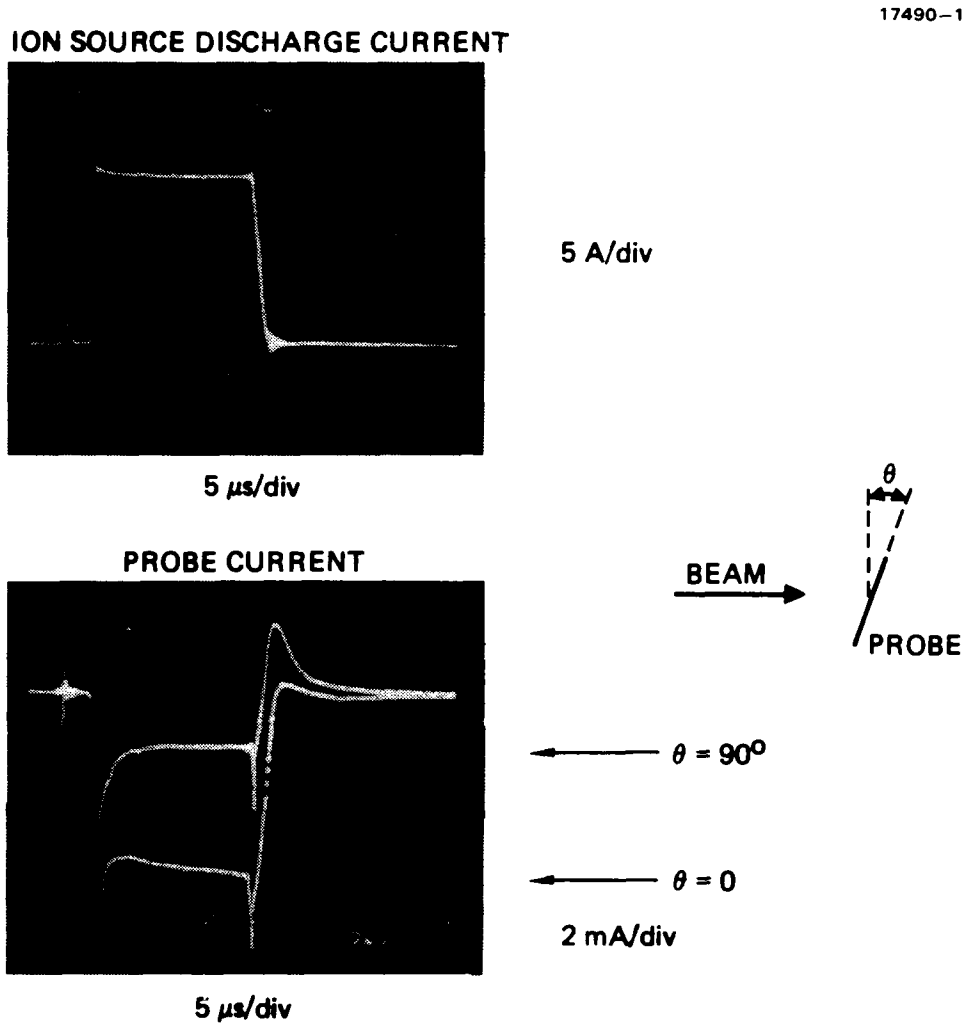

Figure 13. Beam current measured by 1-mm-diameter disk probe.

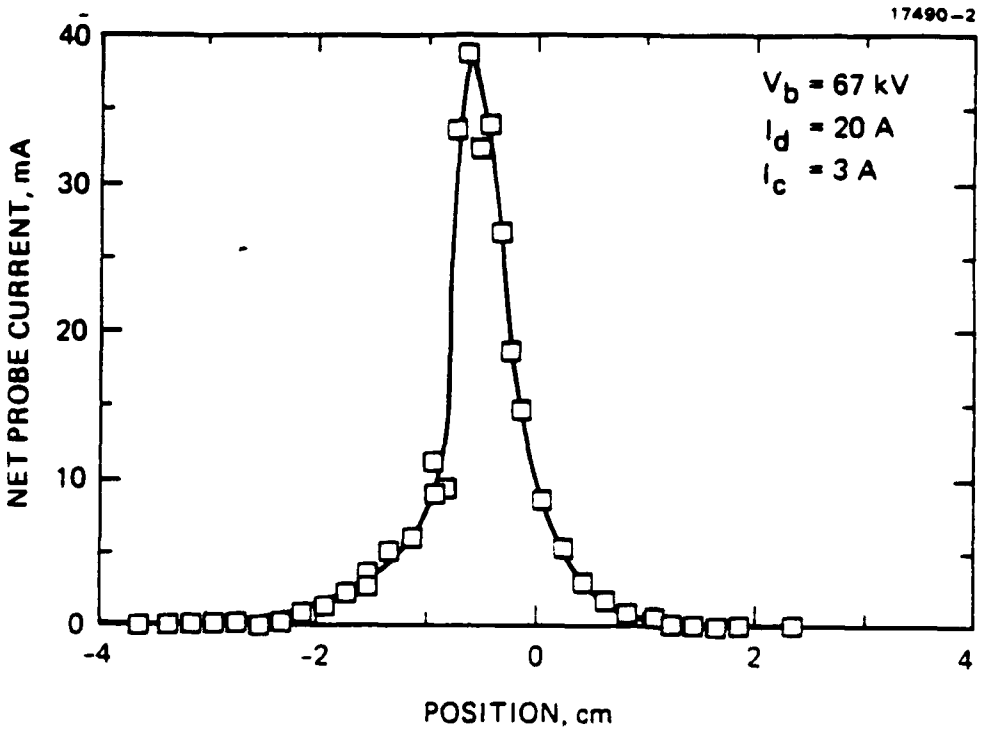

Figure 14. Radial beam profile.

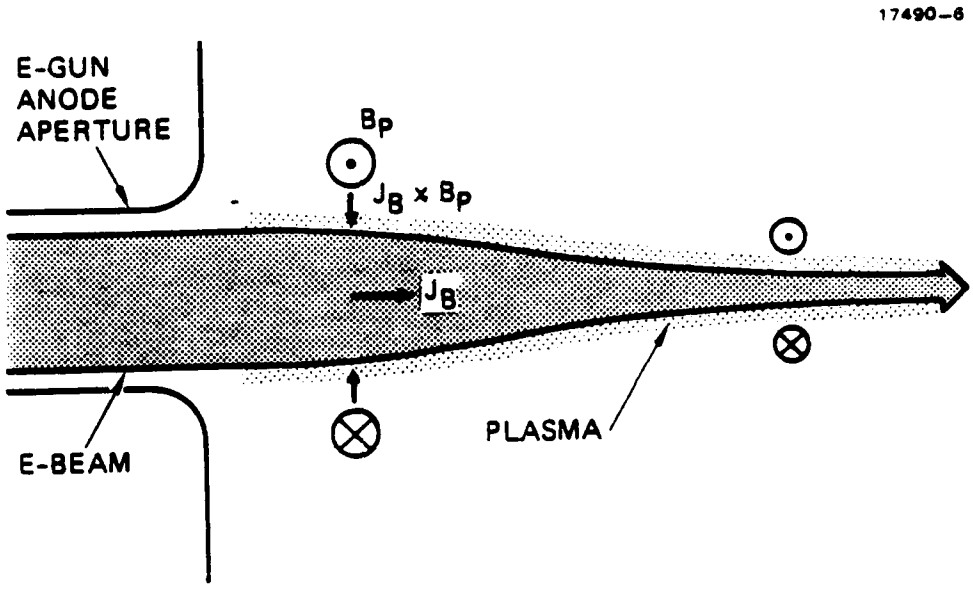

Figure 15. Bennett-pinch effect.

where B_p is the poloidal magnetic field, n_b is the beam density, and $T_{b\perp}$ is the transverse beam temperature. The current at which the pinch occurs can be expressed as

$$I_b^2 \geq 3.2 \times 10^{-10}\, n_b\, A_b\, T_{b_\perp}\ (\text{eV}) \quad , \tag{8}$$

where A_b is the cross-sectional beam area. Under equilibrium conditions where the magnetic-pinch force balances the transverse thermal pressure, theory predicts the beam to maintain the Bennett profile, given analytically by the equation,

$$I_b(r) = \frac{I_{b_o}}{\left[1 + \left(\frac{r}{a}\right)^2\right]^2} \quad , \tag{9}$$

where r is the radial position relative to the center of the beam and a is the Bennett radius given by,

$$a = \frac{2\sqrt{2}\,\lambda_D}{\beta} \left(\frac{T_{b_\perp}}{T_{b_\perp} - T_e}\right)^{1/2} \quad . \tag{10}$$

In this expression, T_e is the background plasma electron temperature, λ_D is the Debye length of the beam plasma, and $\beta = v/c$.

Figure 16 shows a fit comparison of the measured profile at 2.1 A of actual beam current with a curve which corresponds to the Bennett-profile theory. The data points correspond quite well to the Bennett-pinch prediction for a Bennett radius of a = 0.5 cm. Using the measured beam parameters (V_b = 67 kV, I_b = 2.1 A, $n_b = 1.1 \times 10^9$ cm^{-3} and A_b = 0.8 cm^2) and the Bennett radius from the curve fit in Figure 16, we can calculate the transverse beam temperature from Eq. (10). The result is $T_{b\perp}$ = 15 eV which is in rough agreement with the result from the "beam-slit shadowgraph" diagnostic discussed in the next section.

When the ion-source discharge current is increased to values where the ion current becomes space-charge limited, the beam profile broadens significantly. Figure 17 shows such a profile where the discharge current was set to 102 A at a beam voltage of 63 kV. The 7-mm-diameter on-axis beam is still observed, but now broad wings are also obtained which extend many centimeters around the central peak. We believe the wings are generated by the defocusing of the beam by the high ion-space-charge levels near the anode as described earlier.

2.2.5 Direct Beam-Temperature Diagnostic

Cold, high-brightness, low-divergence beams are required for driving advanced systems such as free-electron lasers, E-beam weapons, and excimer lasers. An important parameter which quantifies the quality of an electron beam is the transverse temperature. To accurately determine this beam parameter in the PAG, we have designed a "beam-slit shadowgraph".

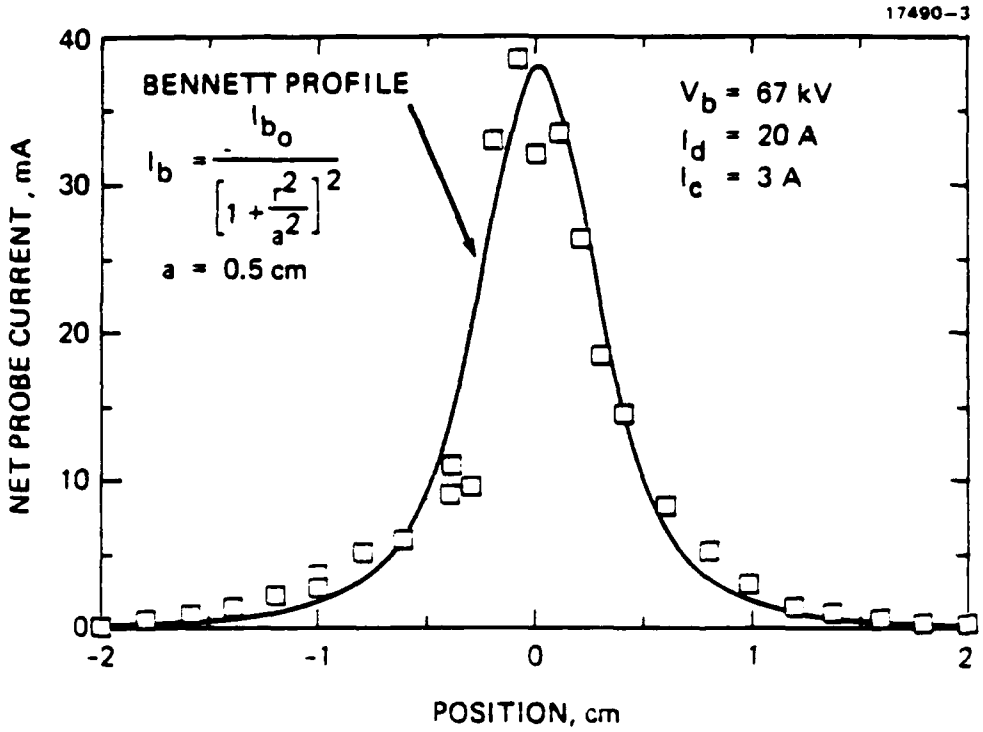

Figure 16. Electron-beam profile is consistent with Bennett-pinch theory.

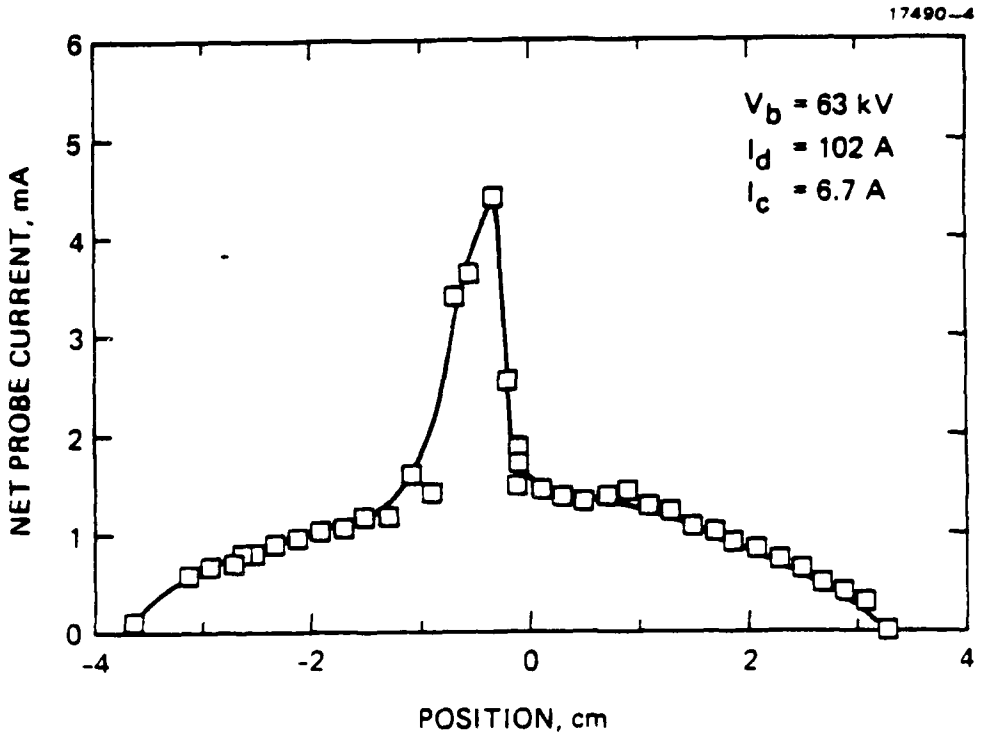

Figure 17. Beam profile with PAG operating in the ion-space-charge current-limited regime.

As shown schematically in Figure 18, the E-beam impinges on the front plate of the shadowgraph which has a narrow slit of size $2L_x$ and $2L_y$ (for the x and y dimensions, respectively). A small portion of the total beam current passes through the slit, drifts through the length of the analyzer, and is collected on an array of wire electrodes mounted on the back plate. By measuring the spatial beam profile at the back plate, we obtain an estimate of the transverse beam temperature.

To readily estimate the transverse beam temperature from the full width of the beam image on the back plate in the x direction, W_x, we use the equation

$$W_x = 2L_x + 2L_z \tan[(T_x/E_b)^{1/2}] \quad , \tag{11}$$

where L_z is the distance between the front and back plates, T_x is the beam temperature in electron volts in the x direction, and E_b is the beam energy in electron volts. For example, if we use $2L_x$ = 1 mm, L_z = 10 cm, T_x = 20 eV, and E_b = 100 keV, we find that W_x = 3.8 mm. The temperature in the y-direction, T_y, can be measured by rotating the analyzer 90° in the x-y plane and repeating the measurement. In this manner the complete two-dimensional transverse beam temperature can be determined.

We performed an experiment to test this diagnostic technique using the setup shown in Figure 19. An aluminum plate with a variable-width molybdenum slit is mounted to a probe shaft. The other probes downstream of the plate are used to measure the

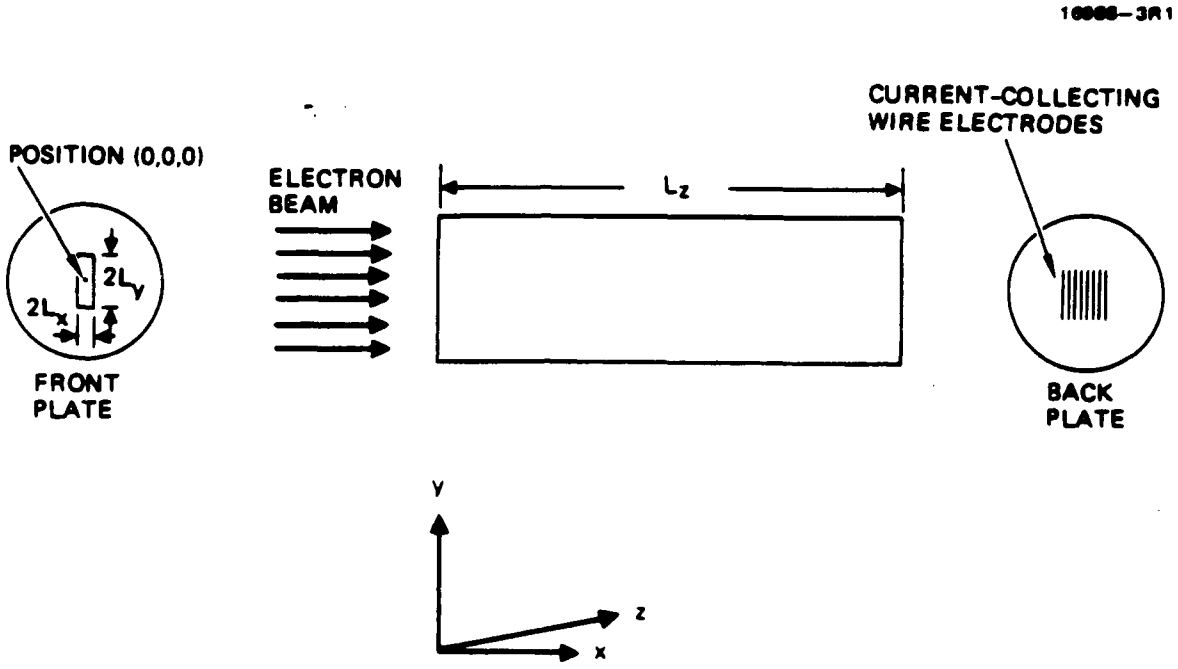

Figure 18. Schematic of the "beam-slit shadowgraph" for measurement of the transverse electron-beam temperature.

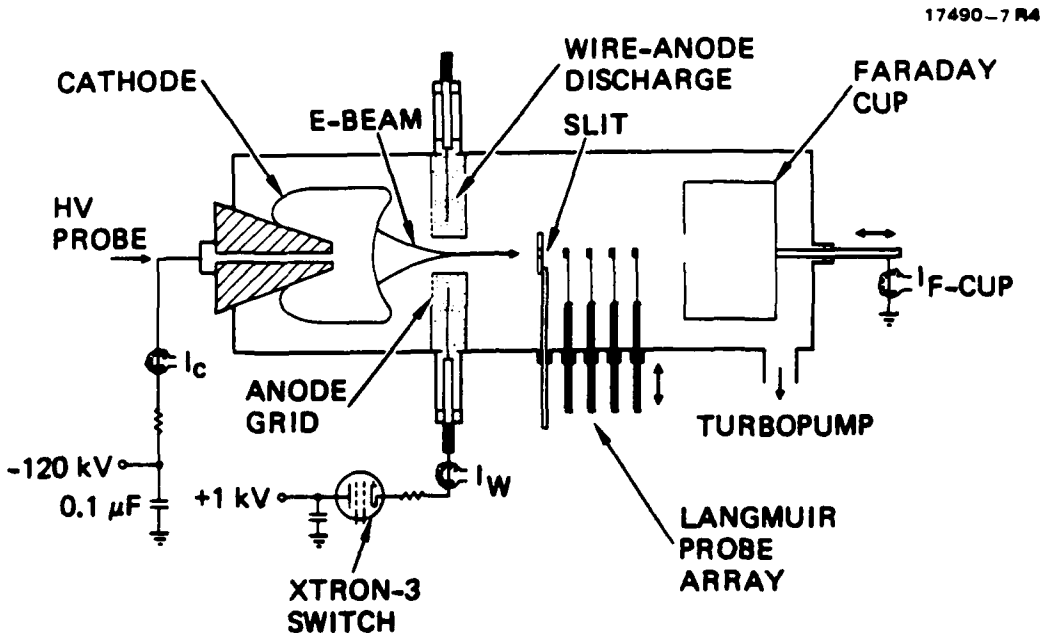

Figure 19. Schematic of the 120-kV PAG scaling experiment with a "beam-slit shadowgraph." The beam slit is located just upstream of the Langmuir-probe array.

current distribution at different distances from the plate. The measured current distribution using a 2-mm-wide slit and a 70-kV, 2.5-A beam is shown in Figure 20. Using the simplified analysis represented by Eq. (11) to estimate the transverse beam temperature we obtain a value of $T_{b\perp}$ = 14 eV – consistent with the result that was obtained from the Bennett-profile fit.

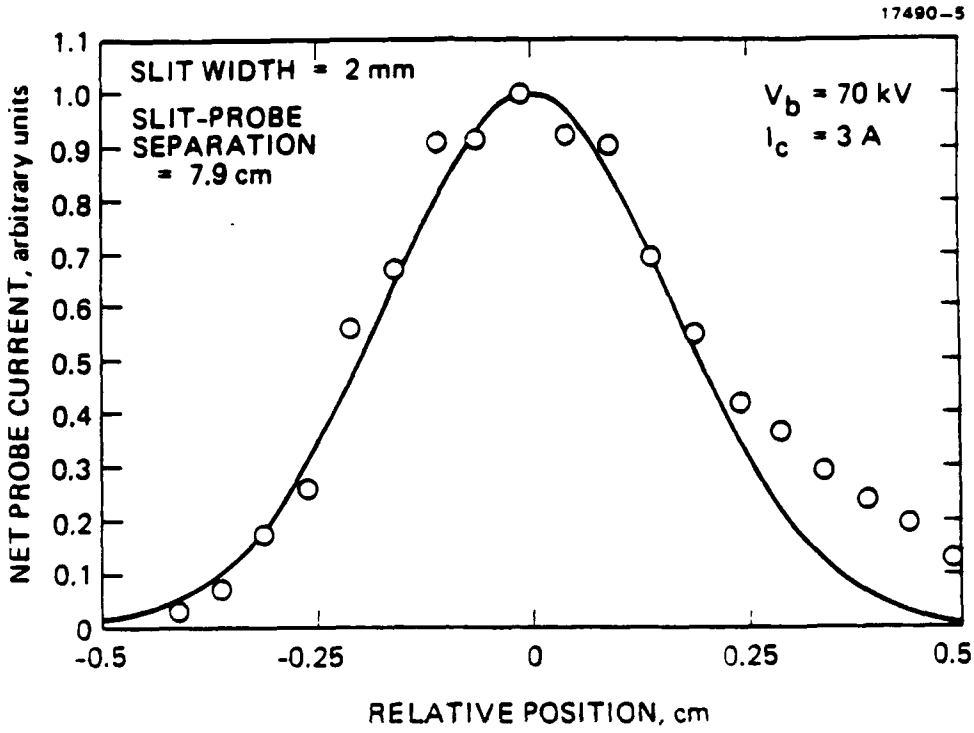

Figure 20. Current distribution measured 7.9 cm downstream of the beam slit.

SECTION 3

HOLLOW-CATHODE-PLASMA E-GUN EXPERIMENTS

Because of the electron-beam current density limitations in the PAG that were discussed in the previous section, we searched for a modified cold-cathode E-gun configuration that would provide significantly higher current density. Under our separate IR&D project on Pulsed Power Switches for Military Systems we rediscovered Hughes plasma-cathode E-gun[9] which was originally invented and developed by R.C. Knechtli as a low current-density ($\leq$1 A/cm^2) rectangular cross-section gun for driving gas-discharge lasers. Plasma cathodes usually have plasma-boundary stability problems, but Hughes plasma E-gun exploited a hollow-cathode discharge to gridded electrode that served as a stabilizing structure as long as the discharge current to the grid was maintained below the electron-beam space-charge-limited current in the accelerating gap.

Under our IR&D project we modified the plasma cathode E-gun to operate at current density up to 40 A/cm^2 in a circular rather than rectangular cross-section configuration in order to exploit its capabilities to drive microwave generators. With the consent of the Air Force, we then adapted the new gun configuration to the requirements of our parallel Plasma Three-Wave-Mixing Program (Air Force Office of Scientific Research Contract No. F49620-85-C-0059) under the present PAG contract. The Three-Wave-Mixing program was previously using planar PAG guns and millimeter-wave power scaling experiments with beam current

were limited to only 7 A of total injected beam current. The adapted plasma-cathode guns have enabled the E-gun current to reach the 100-A level at 30-kV of beam voltage as described below.

3.1 HOLLOW-CATHODE-PLASMA (HCP) E-GUN CONFIGURATION

The new high-current cold-cathode device is called the Hollow-Cathode-Plasma or HCP E-gun because it exploits a low-pressure glow discharge inside a hollow-cathode (HC) enclosure as shown in Figure 21 to generate a stable high-density plasma from which a high-current-density E-beam can be extracted. The enclosure is filled with 5 to 100 mTorr of helium gas which is ionized in a low current (100 mA) keep-alive discharge to a fine-wire anode by a 2-kV power supply as shown in the Figure. The keep-alive plasma provides for low jitter ignition of the high-current discharge which is struck between the hollow cathode and the HC-discharge grid that is located just outside the HC aperture.

The HC configuration with large cathode-to-anode area ratio provides efficient confinement of ionizing electrons inside the HC, and thus enables high-density plasma generation at low gas pressures. The HC plasma is modulated by applying a negative pulse to the HC relative to the anode grid with the HC-discharge pulser, as shown. The HC-discharge grid has a high optical transparency (~62%), yet ultrasmall apertures (~250 μm diameter). The high-density plasma (n_e ~ $3 \times 10^{12}/cm^3$ at 60 A/cm^2 current

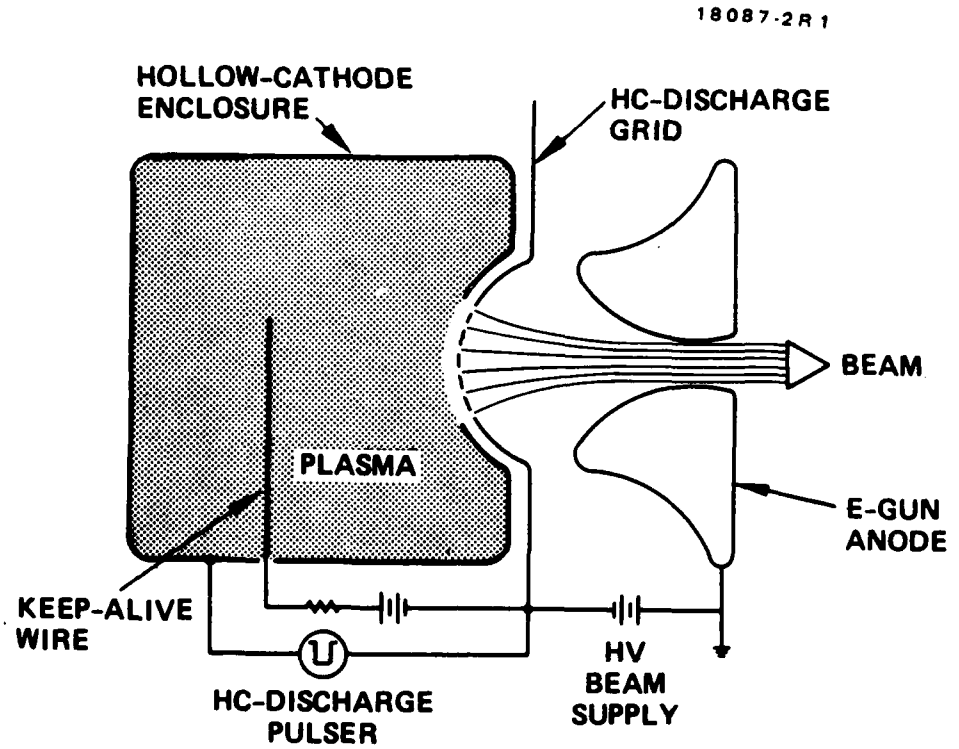

Figure 21. Hollow-cathode-plasma electron-gun configuration.

density) behind the anode-sheath at this grid provides the high-current-density electron emission in the HCP gun. Electrons are extracted from the plasma and accelerated to high energy by applying a high positive potential to the electron-gun anode electrode, which is located to the right of the HC-discharge grid in Figure 21. The beam is electrostatically focused through the aperture in the anode to form a high-current-density, circular-cross-section beam. The plasma surface behind the HC-discharge grid remains stable for arbitrary pulse lengths as long as the HC-discharge current does not exceed the space-charge-limited E-beam current in the accelerating gap. The beam current may be controlled in a linear manner by simply adjusting the current provided by the HC discharge pulser. For high transparency HC-discharge grids, the E-beam to HC-discharge current ratio is nearly one to one.

3.2 HCP E-GUN ADAPTATION FOR THREE-WAVE MIXING

Hughes HCP E-gun design was adapted for high-current beam injection in the AFOSR Millimeter-Wave Generation Via Plasma Three-Wave-Mixing Program by configuring the gun electrodes inside a 4-in.-diameter stainless-steel vacuum tube as shown in Figure 22. The HC is supported inside the tube by an epoxy-casting high-voltage bushing shown to the left in the Figure. The HC is biased to -HV by a capacitor bank through the HV coax cable. The HC-discharge grid is supported by three radially positioned bushings. The anode grid is held at ground

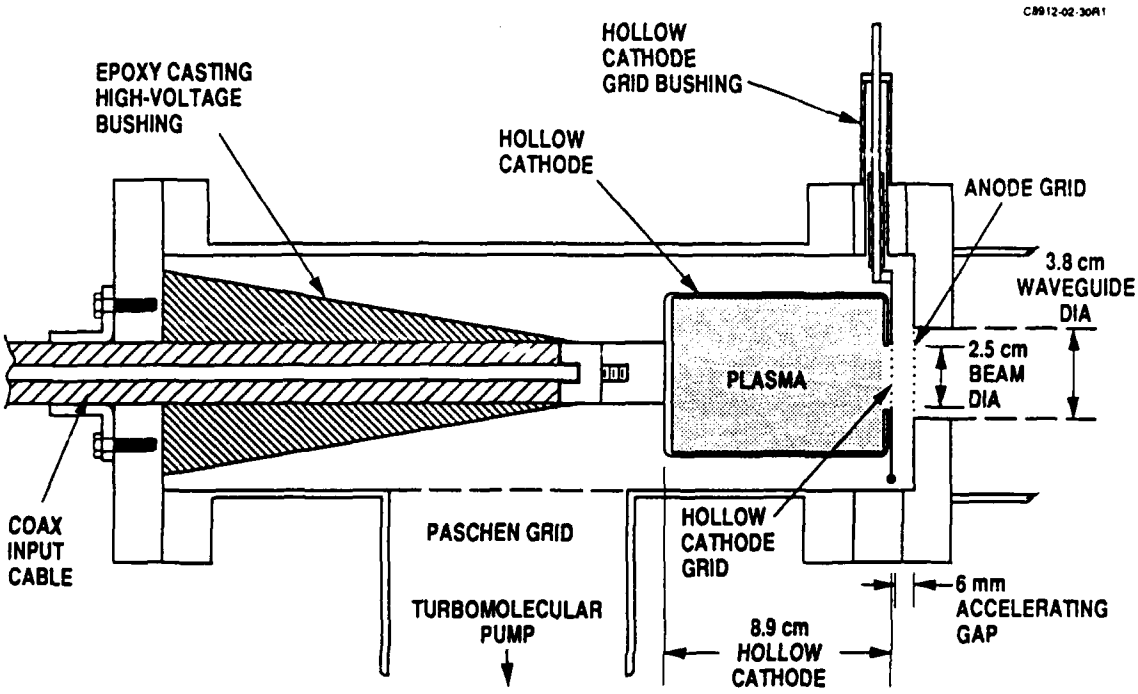

Figure 22. Experimental set-up for testing the high-current HCP E-gun.

potential. This grid also serves as the terminating grid of the 3.8-cm-diameter plasma-filled waveguide cavity into which the beam is injected. The E-beam diameter is defined by the 2.5-cm-diameter aperture in the HC-discharge grid.

The pulsed-power circuit that was assembled to drive the HCP E-gun is shown in Figure 23. A 50-kV power supply charges a 0.5-μF capacitor to supply the -HV for the HC and HC-discharge grid. The HC-discharge pulser is constructed on a corona-shielded floating deck and powered by an isolation transformer since the pulser must float at the -HV beam potential. A square-waveform CROSSATRON-switch modulator is used to generate the HC-discharge pulse. The 5-kV supply charges the floating 3-μF capacitor through a charging diode which is connected across the switch. When the switch is turned on, the capacitor voltage appears on the HC and the discharge is initiated. An 80-Ω series resistor limits the discharge current. Fine adjustments of the discharge current are made by varying the voltage on the 3-μF capacitor.

Figure 24 shows a schematic of the present Three-Wave-Mixing experiment following its upgrade with the addition of two HCP E-guns. The following subsection describes the performance of the E-guns.

3.3 HCP E-GUN PERFORMANCE AND SCALING

The two new HCP E-guns were installed on the Three-Wave-Mixing experiment and tested under the PAG contract. At beam voltages up to 30 kV the current in each E-gun was scaled

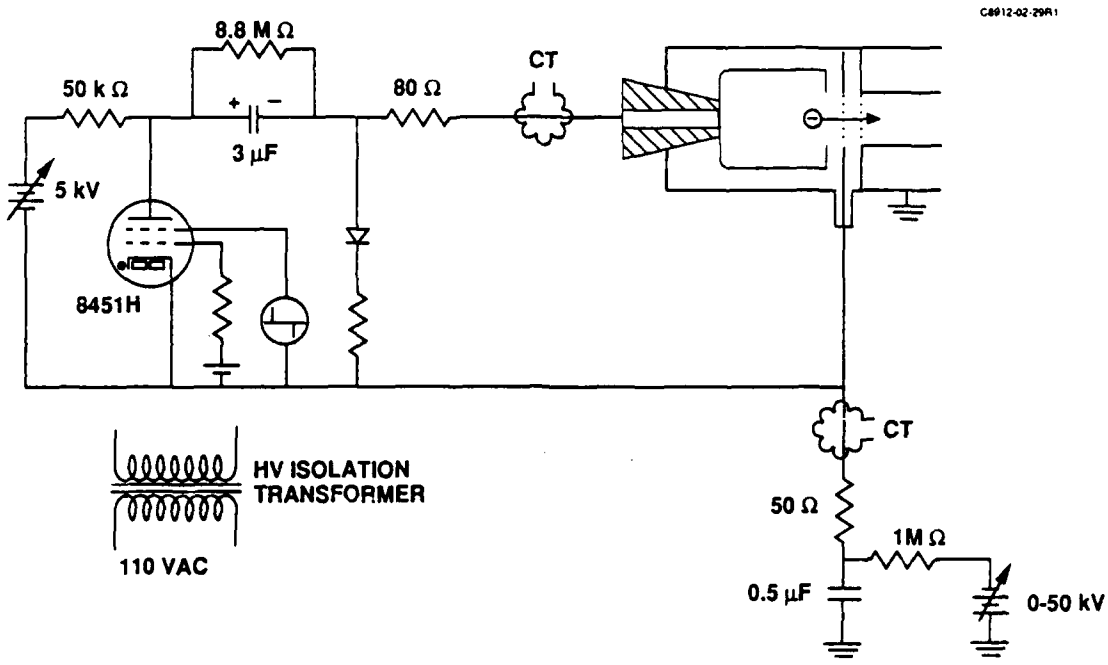

Figure 23. HCP E-gun Pulsed-Power circuit.

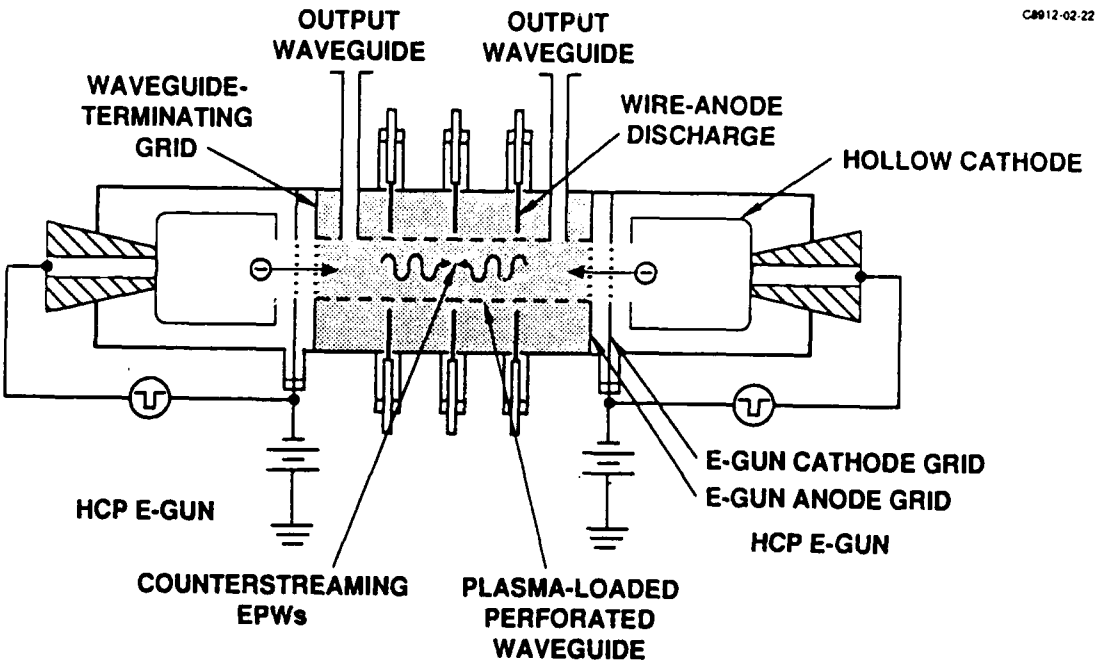

Figure 24. Three-Wave-Mixing experiment driven by HCP E-guns.

up to 100 A by adjusting the HC-discharge to currents slightly above the desired E-beam current level. Figure 25 shows discharge and beam-current waveforms for 13-μs-long pulses at 30 kV of beam voltage. At this current, the injected beam current density is 20 A/cm^2, or more than 10 times that achieved in the plasma-anode E-gun.

The scaling of beam current with HC-discharge current at 30 kV of beam voltage is plotted in Figure 26. The ratio of the two currents is nearly 1 to 1 until the diode-gap space-charge-limiting current is approached at about 100 A.

C8912-02-28R1

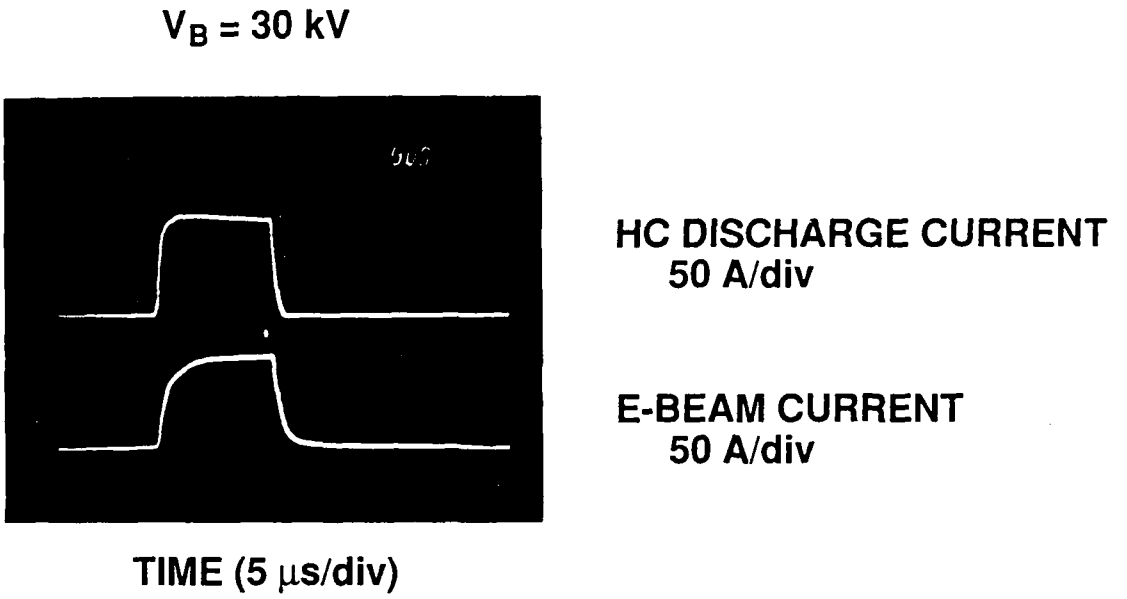

Figure 25. HCP E-gun waveforms.

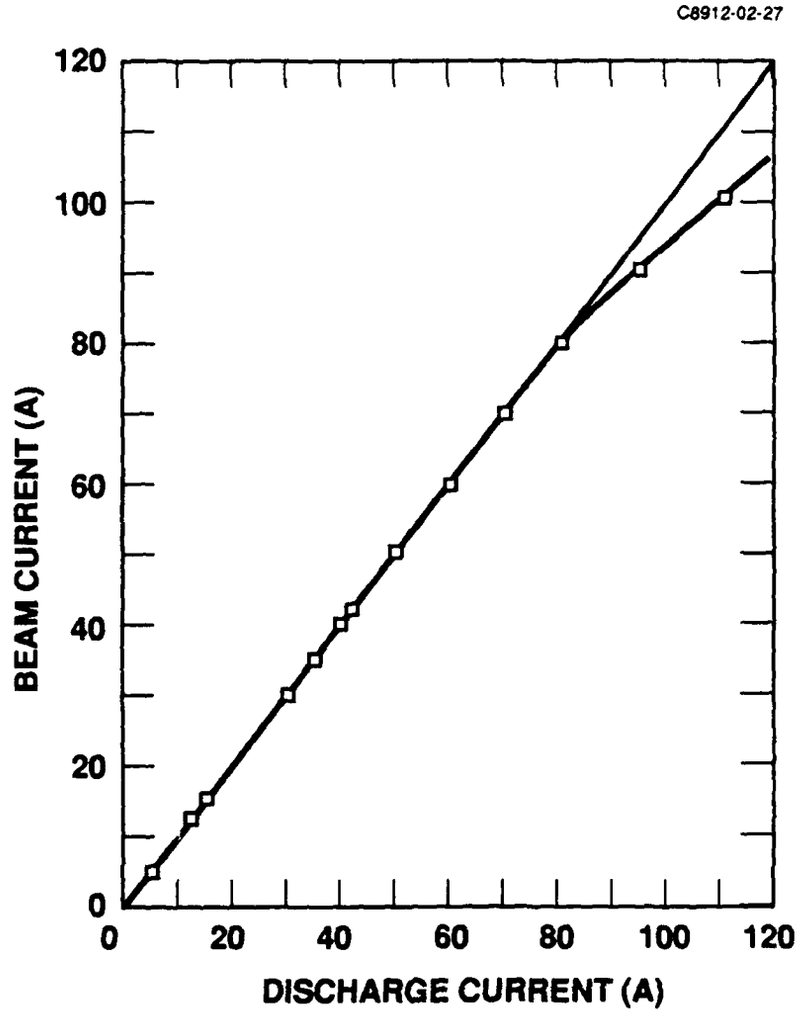

Figure 28. Beam current scaling with HC discharge current.

SECTION 4

INTERACTIONS

A. The following paper was presented at the 1986 American Physical Society Plasma Physics Division Meeting in Baltimore, Maryland on 8 November 1986.

"Plasma-Anode E-Gun," by A.J. Palmer, R.J. Harvey, R.W. Schumacher, F.A. Dolezal, D.J. Gregoire, and J. Santoru.

B. The following paper was presented at the IEEE International Conference on Plasma Science on 2 June 1987 in Arlington, Virginia.

"Plasma-Anode e-Gun," by J. Santoru, R.W. Schumacher, A.J. Palmer, R.J. Harvey, F.A. Dolezal, and D.J Gregoire.

C. A seminar on the PAG was given at the Naval Research Laboratory in Washington, D.C., on 5 December 1986.

D. The following paper was presented at the 1987 APS Division of Plasma Physics Meeting on 2 November 1987 in San Diego, California.

"Plasma-Anode Electron Gun (PAG) Scaling," by J. Santoru, R.W. Schumacher, R.J. Harvey, and A.J. Palmer.

E. The following paper was presented at the 1989 IEEE Conference on Plasma Science on 24 May 1989 in Buffalo, New York.

"Millimeter-Wave Radiation Generated Via Plasma Three-Wave Mixing Using High-Current Density Counterstreaming Electron Beams," by J. Santoru and R.W. Schumacher.

SECTION 5

PUBLICATIONS

"Plasma-Anode Electron Gun," to be submitted to Journal of Applied Physics

SECTION 6

RESEARCH PERSONNEL

The following personnel at Hughes Research Laboratories are associated with the research effort:

1. Robert W. Schumacher (Principal Investigator)
   Project Manager (213) 317-5439

2. Joseph Santoru
   Member of the Technical Staff (213) 317-5838

3. Allan J. Palmer
   Member of the Technical Staff (213) 317-5710

4. Ronnie M. Watkins
   Development Engineer, Specialist (213) 317-5424

5. Robin J. Harvey
   Senior Scientist (213) 317-5236

REFERENCES

1. W.B. Herrmannsfeldt, SLAC Report No. 226, November 1979.

2. R.J. Harvey, "Plasma-Anode Electron Gun," Hughes Aircraft Company patent disclosure No. 84050, U.S. patent pending.

3. J.R. Pierce, Theory and Design of Electron Beams, 2nd Ed., Van Nostrand, New York, 1954.

4. G.W. McClure, "Low-Pressure Glow Discharge," Appl. Phys. Lett. 2, No. 12, 233 (1963).

5. J.R. Bayless and R.J. Harvey, "Continuous Ionization Injector for Low-Pressure Gas-Discharge Device," U.S. Pat. No. 3, 949, 260 (1976) [Assigned to Hughes Aircraft Company].

6. P.F. Little, "Secondary Effects," Band XXI, Vol. XXI, Handbook der Physics (1956). Also see A.G. Hill et al., Phys. Rev. 55, 463-470, March 1939.

7. H.E. Gallagher and R.J. Harvey, "Development of 1-GW Electron Beam Controlled Switch," IEEE Conf. Record 1984 Sixteenth Power Modulator Symposium, June 1984, p. 158.

8. W.H. Bennett, Phys. Rev. 45, 890 (1934); also see N.A. Krall and A.W. Trivelpiece, "Principles of Plasma Physics," p. 495, McGraw Hill, New York (1973).

9. R.C. Knechtli, U.S. Patent No. 3,831,052 (1974).